Nano Energy (2015) 12, 96–104

Available online at www.sciencedirect.com

ScienceDirect

journal homepage: www.elsevier.com/locate/nanoenergy

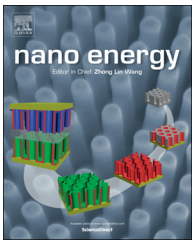

RAPID COMMUNICATION

Highly efficient and stable planar perovskite solar cells with reduced graphene oxide nanosheets as electrode interlayer

Jun-Seok Yeo[a], Rira Kang[a], Sehyun Lee[a], Ye-Jin Jeon[a], NoSoung Myoung[b], Chang-Lyoul Lee[b], Dong-Yu Kim[a,*], Jin-Mun Yun[c], You-Hyun Seo[d], Seok-Soon Kim[e], Seok-In Na[d,**]

[a]*Heeger Center for Advanced Materials (HCAM), School of Materials Science and Engineering, Gwangju Institute of Science and Technology, Gwangju, 500-712, Republic of Korea*
[b]*Advanced Photonics Research Institute (APRI), Gwangju Institute of Science and Technology, Gwangju, 500-712, Republic of Korea*
[c]*Radiation Research Division for Industry and Environment, Korea Atomic Energy Research Institute (KAERI), 29 Geumgu-gil, Jeongeup-si, Jeollabuk-do, 580-185, Republic of Korea*
[d]*Professional Graduate School of Flexible and Printable Electronics and Polymer Materials Fusion Research Center, Chonbuk National University, Jeonju-si, Jeollabuk-do, 561-756, Republic of Korea*
[e]*School of Materials Science and Chemical Engineering, Kunsan National University, Kunsan, Chonbuk, 753-701, Republic of Korea*

Received 15 October 2014; received in revised form 1 December 2014; accepted 14 December 2014
Available online 23 December 2014

KEYWORDS
Perovskite solar cells;
Reduced graphene oxides;
Planar structures;
Interlayers

Abstract
We demonstrate a simple solution and room-temperature processed reduced graphene oxide (RGO) as a novel hole-transporting material (HTM) to guarantee highly efficient and highly stable $CH_3NH_3PbI_3$ perovskite solar cells (PeSCs). The effects of RGO HTM are systemically investigated in terms of PeSC efficiency, PeSC stability, morphology of perovskite film, recombination dynamics, and charge-transport through $CH_3NH_3PbI_3$/HTM interface. The resultant PeSC with a planar configuration of glass/ITO/RGO/$CH_3NH_3PbI_3$/$PC_{61}BM$/bathocuproine (BCP)/Ag exhibits improved device efficiency (maximum PCE of 10.8%) with high reproducibility than those of the reference devices using conventional PEDOT:PSS and GO HTMs. Also, the RGO-based PeSCs show highly desirable device stability in comparison to the PEDOT:PSS PeSCs.

*Corresponding author. Tel.: +82 62 715 2319; fax: +82 62 715 2304.
**Corresponding author. Tel.: +82 63 270 4465; fax: +82 63 270 2341.
E-mail addresses: kimdy@gist.ac.kr (D.-Y. Kim), nsi12@jbnu.ac.kr (S.-I. Na).

http://dx.doi.org/10.1016/j.nanoen.2014.12.022
2211-2855/

Introduction

Organic-inorganic perovskites employing methylammonium lead halide hold great promise for use as light harvesters in the field of next-generation photovoltaics, and this can be ascribed to their competitive efficiency and low-cost manufacturing [1-8]. The high levels of interests and research activities involving perovskite solar cells (PeSCs) have resulted in great progress in power conversion efficiency (PCE) – more than 17% – in a very short timescale [9-12]. However, the breakthroughs in PCEs for PeSCs have been achieved mostly by the incorporation of dye-sensitized solar cell architectures that typically require high-temperature processing due to the use of metal oxides as charge-transporting materials, which is one of the big challenges for the market entry of PeSCs. To circumvent these issues, other device configurations based on organic photovoltaic (OPV) structures are being explored for various advantages such as the fabrication through simple and low-temperature processes with flexible formats [4,13-15]. General PeSCs using OPV structures are composed of an indium tin oxide (ITO) anode, poly(ethylenedioxythiophene):poly(styrene sulfonate) (PEDOT:PSS) as a hole-transporting layer, the perovskite layer as a light absorber, [6,6]-phenyl-C_{61}-butyric acid methyl ester ($PC_{61}BM$) as an electron-transporting material (ETM), and a low work function (WF) metal as a cathode. Among these layers, the hole-transporting and electron-transporting layers play a key role in determining the resultant device performance because the heterojunction between perovskite absorbers and adjacent layers could manipulate the p-i-n characteristics and charge extraction performances in the PeSCs [9,16-18].

The efforts to optimize the heterojunction of electron-transporting layer/perovskite have mostly focused on the fullerene derivatives since, as verified by several reports, the electron charge transfer from perovskites to fullerenes is both very fast (~0.4 ns) and efficient (92%) in the illumination state, thus, fullerene materials have been recognized as the perfect electron quenchers [4,19,20]. Jeng et al. applied fullerene derivatives as electron acceptors with diverse lowest unoccupied molecular orbital (LUMO) levels and demonstrated that the interface of $CH_3NH_3PbI_3$ perovskite/fullerene could control photovoltaic performances with energy-level alignments [15]. Also, the effect of controlling $PC_{61}BM$ film thickness on device performances has recently been reported for PeSCs [21]. Unlike the intense interests in efficiency enhancements associated with the evolution of various fullerene derivatives and the optimization of process conditions that are noted above, very little interest has been paid to the efforts on hole-transporting materials (HTMs) in PeSCs based on OPV structures, although the efforts on searching other HTMs are as important as those of the electron-transporting materials in the enhancement of PeSC performance. Furthermore, almost exclusively used PEDOT:PSS HTM should be replaced due to the detrimental effects of its hygroscopicity and acidity on device durability as widespread acceptance.

Recently, nickel oxides have been demonstrated as an alternative to PEDOT:PSS as a hole-transporting layer in PeSCs with better energy-level alignments between $CH_3NH_3PbI_3$ perovskites and nickel oxides [22,23]. However, to achieve a reasonable PCE, the nickel oxide required either a high-temperature process or a vacuum-process and additional UV/O_3 treatment, which can nullify the solution-processible manufacturing of PeSC based on OPV structures. Also, although very recent accomplishment of the solution-processible graphene oxide (GO) as an alternative HTM was demonstrated in PeSC with OPV architecture employing a $CH_3NH_3PbI_{3-x}Cl_x$ absorber [24], the GOs could have their intrinsic disadvantages for HTMs such as an insulating property and a high degree of oxygen contents on their surfaces [25]. Furthermore, the important issues on PeSCs with alternative HTMs to PEDOT:PSS remain concerning the charge-transfer behaviors through a perovskite interlayer, and concerning the device stability of PeSCs. Thus, greater interest in hole-transporting materials should be devoted for development of higher efficiency, increased cost-effectiveness, and more stable perovskite solar cells.

The present study is the first to demonstrate how solution-based reduced graphene oxide (RGO) films processed at room temperature can dramatically raise the device performance of perovskite-based solar cells. As a novel electrode interlayer in PeSCs, we used RGO reduced through p-hydrazinobenzenesulfonic acid hemihydrate, because this RGO satisfies most of the requirements of an ideal HTM in terms of low cost, abundance, solution processibility, conductivity, and stability [25,26]. In particular, recently developed RGOs have shown an enhanced conductivity and a higher work function than conventional PEDOT:PSS and hydrazine-based RGOs [26]. Here, we combined $CH_3NH_3PbI_3$ light absorbers with an ultra-thin RGO, and we systemically studied the effects of RGO HTM in terms of PeSC efficiency, PeSC stability, morphology of perovskite film, recombination dynamics, and charge transport through $CH_3NH_3PbI_3$/HTM interface. As a result, a PeSC with a configuration of glass/ITO/RGO/$CH_3NH_3PbI_3$/$PC_{61}BM$/bathocuproine (BCP)/Ag exhibited better device efficiency (maximum PCE of 10.8%) with high reproducibility than those of the reference devices using PEDOT:PSS and GO HTMs. Furthermore, the RGO-based PeSCs showed highly desirable device stability in comparison to the conventional PEDOT:PSS PeSCs. This promising strategy will be a critical step toward the ideal HTM design for the advancement of practical perovskite solar cells.

Results and discussion

The PeSC configuration and the chemical structure of RGO used as a HTM are illustrated in Fig. 1(a). Aqueous suspensions of RGO with outstanding dispersibility presented simple fabrication technique with no thermal treatments, and resulted in a thin hole-transporting layer with a thickness of about 3 nm on ITO glass substrates. $CH_3NH_3PbI_3$ perovskite film for use as a light harvester was grown by recently developed solvent additive process by using a small amount of N-cyclohexyl-2-pyrrolidone (CHP), which resulted in a highly uniform and flat surface of the perovskite film, thereby leading to highly reproducible PeSC performances [27]. Then, an optimized 100 nm-thick $PC_{61}BM$ layer and BCP/Ag cathodes

covered $CH_3NH_3PbI_3$ perovskite layers. Fig. 1(b) for the cross-section image of scanning electron microscopy (SEM) shows the well-fabricated and uniform structure of planar PeSC with RGO HTMs. The corresponding energy diagram of each layer is shown in Fig. 1(c). Recent reports have alluded that minimizing the mismatch between the energy levels of perovskite and transporting materials promotes the transfer of charge carriers and elevates the voltage output [9,16,22,28]. Accordingly, the 0.3 eV higher WF of RGO HTMs relative to PEDOT:PSS HTMs as provided in Fig. S1 can be anticipated to show desirable charge transfer across the heterojunction of RGO/$CH_3NH_3PbI_3$ perovskite with minimal energy losses and minimal degradations in the photovoltage of PeSCs.

In order to explore the potential of the RGO as HTMs in PeSCs, we first evaluated the optical properties of $CH_3NH_3PbI_3$ perovskite layers on ITO/RGO films. PEDOT:PSS and GO before reduction were chosen as HTMs for a comparative study. In the optical absorption shown in Fig. 2(a), the ability of light harvesting for each of the $CH_3NH_3PbI_3$ perovskite film was similar, and no noticeable transition of the absorption pattern was obtained over the entire visible spectrum, regardless of a variety of HTM types. For further examination on the compatibility of RGO HTMs within the perovskites devices, we measured the steady-state photoluminescence (PL) spectra. Fig. 2(b) provides the PL characteristics of $CH_3NH_3PbI_3$ perovskites layers on ITO/PEDOT:PSS, ITO/GO, and ITO/RGO substrates. The intensity of the PL response from the $CH_3NH_3PbI_3$ perovskite film was reduced on the order of PEDOT:PSS, GO, and RGO. We noted that when the almost equal magnitude of absorbance among the three types of HTMs was accounted for, the RGO exhibited the best PL quenching ability, and the holes generated in perovskites absorbers could be more efficiently transferred into RGO HTMs compared to conventional PEDOT:PSS HTMs [4].

To directly access the performance of RGO as a contact material for $CH_3NH_3PbI_3$ perovskites, we fabricated the planar PeSCs with an OPV-based configuration on ITO substrates using different HTMs: PEDOT:PSS (~30 nm), GO (~3 nm), and RGO (~3 nm). The detailed statistics and averaged photovoltaic parameters are summarized in Fig. S2 and Table 1. Also, to confirm the accurate characterization of PeSCs in this study, their corresponding hysteresis properties of the photocurrents were measured according to the previous reports as shown in Fig. S3 and S4 [11,29]. Encouragingly, the PeSCs employing RGO HTMs presented the PCE enhancement by ca. 20% relative to conventional devices using PEDOT:PSS as shown in Fig. 2(c) and (d). The representative photovoltaic parameters of the device using RGO HTM showed an open-circuit voltage (V_{OC}) of 0.98 V, a short-circuit current density (J_{SC}) of 15.4 mA cm^{-2}, a fill factor (FF) of 71.6%, and a PCE of 10.8%, whereas the control device incorporating PEDOT:PSS exhibited a V_{OC} of 0.91 V, a J_{SC} of 14.1 mA cm^{-2}, a FF of 70.8%, and a PCE of 9.1%. Interestingly, however, when the GO was employed as a HTM, where a main chemical structure of GO is also based on a graphene basal plane like as RGO, a completely inferior performance to that of the RGO in all photovoltaic parameters was observed as follows: a V_{OC} of 0.88 V; a J_{SC} of 11.9 mA cm^{-2}; a FF of 38.5%; and, a PCE of 4.0%. This result could be originated from the electrically insulating properties of GO and the large potential of charge traps due to the oxygenated functionalities and vacancies on the GO sheets [25].

To improve the comparative investigation, we calculated the series resistance (R_s) and the shunt resistance (R_{sh}) from the photocurrent density-voltage (J-V) curves. We observed a reduced R_s of 0.92 Ω cm^2 in the RGO device compared to the PEDOT:PSS device (1.10 Ω cm^2), implying a superior charge-transport ability of RGO, which was probably due to a higher conductivity (~3 S cm^{-1}) and a higher WF than those of PEDOT:PSS HTMs. More importantly, an unexpected shunt

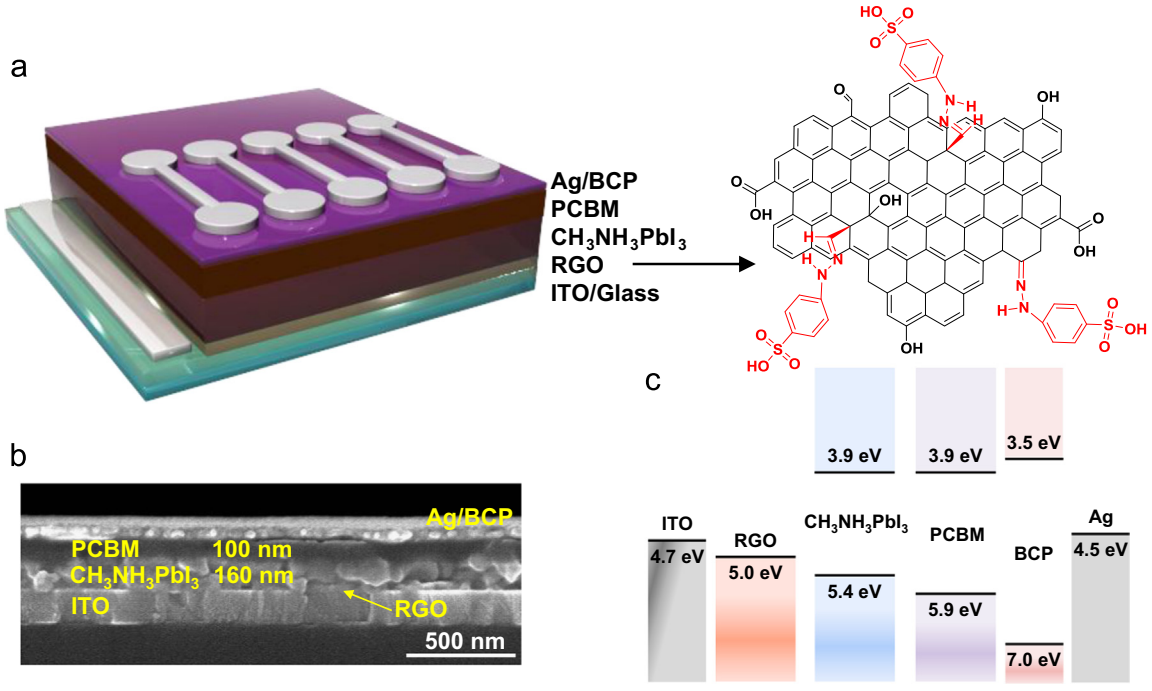

Fig. 1 (a) Schematic PeSC architecture employing a RGO HTM and the chemical structure of RGO used in this study. (b) The cross-sectional SEM image of the resultant device and (c) the corresponding energy-level diagram of each layer.

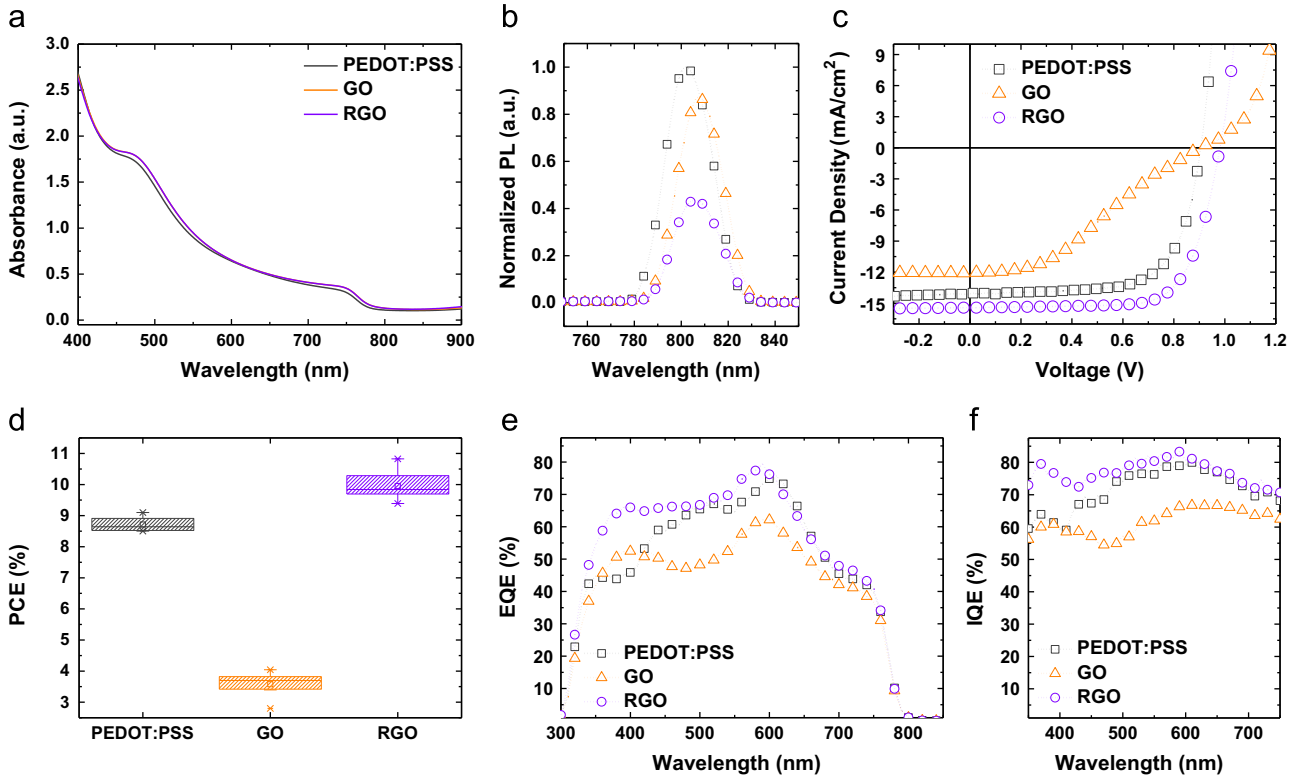

Fig. 2 (a) UV-vis absorption spectra and (b) photoluminescence responses of $CH_3NH_3PbI_3$ films on glass/ITO/PEDOT:PSS, glass/ITO/GO, and glass/ITO/RGO. (c) The representative J-V curves for PeSCs with various HTMs and (d) corresponding PCE statistics based on 20 devices. (e) External quantum efficiency and (f) internal quantum efficiency of different PeSCs.

Table 1 Photovoltaic parameters with average values for PEDOT:PSS, GO, and RGO-based PeSCs.

HTM	V_{OC} (V)	J_{SC} (mA cm^{-2})	FF (%)	PCE (%)	R_s[a] (Ω cm^2)	R_{sh}[a] (kΩ cm^2)
PEDOT:PSS	0.92	13.65	69.97	8.80 ($_{max.}$ 9.14)	1.10	1.65
GO	0.89	10.70	37.61	3.58 ($_{max.}$ 4.04)	3.15	2.41
RGO	0.95	14.81	71.13	9.95 ($_{max.}$ 10.80)	0.92	2.95

[a]The series resistance and the shunt resistance were calculated from illuminated J-V plots converging to V_{OC} and J_{SC}, respectively.

resistance (2.95 Ω cm^2) of the RGO device that was higher than that of the PEDOT:PSS device (1.65 Ω cm^2) was also obtained, suggesting that carrier recombination could be more efficiently blocked through the RGO/perovskites heterojunction than through the PEDOT:PSS/perovskites. This observation is in good agreement with the dependence of V_{OC} on the light intensity as shown in Fig. S5. The PeSC incorporating RGO exhibited a weaker dependence of V_{OC} on the light intensity with a slope of 1.24 kT/e than that of the device using PEDOT:PSS with a slope of 1.89 kT/e, which indicates that the strength of recombination was significantly reduced in the RGO device compared to the PEDOT:PSS device [13,30,31]. It is worth pointing out that the ultra-thin and conducting reduced graphene oxide layer on ITO can be not only an efficient hole-transporting layer but also a favorable electron-blocking layer, which has been generally achieved through the insertion of additional processes and materials such as a fullerene self-assembled monolayer, organic molecules with long alkyl chains, and insulating polymers onto conventional transporting materials [32-34].

The external quantum efficiency (EQE) and internal quantum efficiency (IQE) confirmed the enhanced photocurrent of the RGO device, as shown in Fig. 2(e) and (f). Also, all the calculated J_{SC} values using EQE data were within a 3% error with the corresponding J_{SC} values detected in the J-V curves. The PeSC using RGO showed high and broad spectral responses in wavelength from 300 nm to 800 nm with a maximum peak approaching an 80% value of EQE. Furthermore, the IQE spectrum of RGO cells depicted higher values in the overall wavelength range compared to the reference PEDOT:PSS spectrum, indicating that the efficiency of photon-to-electron conversion was more advanced in the RGO device than the control device even with similar absorption ability using equal light harvesters and their similar optical transparency shown in Fig. S6 [35].

To further unveil the effects of RGO incorporation on the $CH_3NH_3PbI_3$ perovskite devices and possible correlation with enhanced device performances, the morphological changes of the perovskite films on different substrates (ITO/PEDOT:PSS

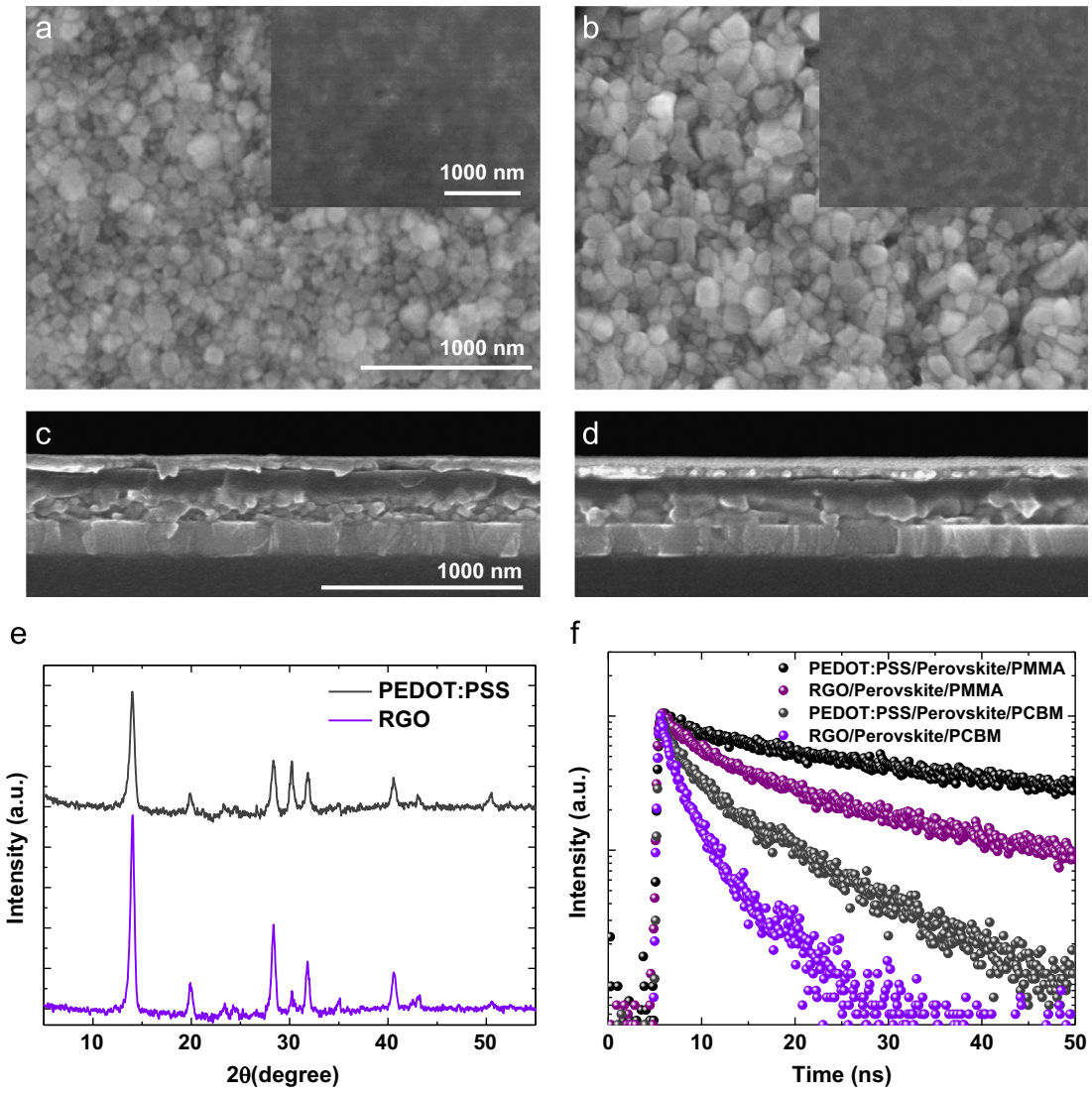

Fig. 3 Top-view SEM images of $CH_3NH_3PbI_3$ films on (a) glass/ITO/PEDOT:PSS, and (b) glass/ITO/RGO. The each inset image shows the SEM image for the corresponding surface of glass/ITO/HTM/$PC_{61}BM$ layer. Cross-sectional SEM images of complete devices with (c) PEDOT:PSS and (d) RGO. (e) XRD patterns of $CH_3NH_3PbI_3$ films on different HTMs with glass/ITO substrates. (f) Time-resolved PL characteristics of the $CH_3NH_3PbI_3$ films based on different HTMs.

and ITO/RGO) were investigated using a series of SEM and X-ray diffraction (XRD) analyses, and the surface morphology for each substrate obtained by atomic force microscopy (AFM) was also shown in Fig. S7. All samples were fabricated using procedures identical to those of working devices. As can be seen in the topview SEM images of Fig. 3(a) and (b), both films grown on ITO/PEDOT:PSS and ITO/RGO exhibited densely covered and well-crystallized cubic structures of $CH_3NH_3PbI_3$ perovskites, which ensure the uniform coverage of upper $PC_{61}BM$ layer. The cross-sectional images in Fig. 3(c) and (d) confirm again a compact morphology and an uniform film thickness of 160 nm without any pin-holes across the entire region in both films, which prevents direct contact between the $PC_{61}BM$ layer and the HTMs to induce an electrical shunting [14,21]. More notably, the grain size was the most distinguishing morphological characteristics of the two types of samples. The enlarged perovskite grains in the range of 100–200 nm were observed in the perovskite film grown on RGO compared to the perovskite film grown on PEDOT:PSS with grain size below 100 nm. The larger size of the perovskite grains resulted in a reduction in the total number of grain boundaries (GBs) in a given volume as can be seen in the SEM images. Very recently, it was found that the GBs in perovskite film could activate a charge recombination owing to their higher surface potential and defect states [10,29,36]. In this respect, the reduced number of GBs shown in RGO HTMs are believed to facilitate the flow of charge carrier with a minimal recombination loss through the GBs. The improved morphology of the $CH_3NH_3PbI_3$ perovskite film on an RGO layer is also evident in the corresponding XRD patterns shown in Fig. 3(e). Stronger reflection peaks of the perovskite structure were clearly obtained in the case of RGO HTMs where peaks of 14.1°, 28.4°, and 31.7° are assigned to (1 1 0), (2 2 0), and (3 1 0) crystal planes of the $CH_3NH_3PbI_3$ perovskites [11]. In particular, the smaller full-width-at-half-maximum (FWHM) of (110) XRD peak (0.49) shown in Fig. S8 represents the better textured domains with a preferred in-plane orientation to substrates, suggesting that the RGO/perovskites interface

could encourage a high degree of crystallinity and texturing [10].

To further examine the influence of RGO on the charge dissociation and recombination processes, we performed time-resolved photoluminescence (TRPL) as shown in Fig. 3(f). We analyzed the PL curves with a bi-exponential decay function including a fast decay (τ_1) component and a slow decay (τ_2) component, and the detailed parameters are summarized in Table 2. The fast decay would be originated from the quenching of charge carriers, meaning that the free carriers generated from the perovskite region were transported to the respective hole or electron contact, and the slow decay component could be attributed to the radiative recombination of free charge carriers before the charge collection [14,36]. In the case of the PEDOT:PSS/$CH_3NH_3PbI_3$ perovskite, the fast decay lifetime of 5.16 ns with a 0.26 fraction and the slow decay lifetime of 47.95 ns with a 0.48 fraction were detected, which suggests that the depopulation of photogenerated charges was dominated by radiative recombination rather than by an appropriate charge collection through the PEDOT:PSS/perovskite interface. In contrast, for the RGO/$CH_3NH_3PbI_3$ perovskite film, the fast decay lifetime and the slow decay lifetime were both shortened (4.44 ns and 26.92 ns, respectively) and the fraction of the fast decay process was much more enhanced than the reference of PEDOT:PSS HTMs, which can be interpreted that the RGO/$CH_3NH_3PbI_3$ perovskite junction could induce a faster charge transfer across its interface with a reduced recombination strength. Furthermore, when the perovskite film forms the junction with $PC_{61}BM$ in addition to RGO, closely resembling the working devices, both types of decay lifetimes were further decreased with negligible fraction of the slow decay component. Therefore, in the case of RGO HTMs, it was apparent that the majority of charge carriers generated under illumination were swept to the respective contacts with minimal recombination, while the recombination process still takes some degree of fraction in PEDOT:PSS HTMs even with a $PC_{61}BM$ electron quencher. The fast charge transfer and collection shown in RGO-based devices may be closely related to the high conductivity, the better-aligned energy levels, the improved morphology such as the reduced GBs, and the high quality of the crystal phase as discussed above, thus contributing to an enhancement of the photovoltaic parameters under working conditions.

To further demonstrate the potential of RGO HTMs, we recorded the device performance as a function of exposure time to ambient conditions with a humidity of approximately 50% without encapsulation according to the ISOS-D-1 protocol [37]. As evident in Fig. 4, the device efficiency of PEDOT:PSS-based cells was drastically deteriorated and showed complete failure in photovoltaic characteristics with 0% just after 120 h of exposure. It is generally acknowledged that a device incorporating PEDOT:PSS is degraded mostly by the erosion of ITO electrodes [26]. In addition to damaged ITO electrodes, for these $CH_3NH_3PbI_3$ perovskite devices, the hygroscopic and highly acidic properties of PEDOT:PSS can activate the decomposition of $CH_3NH_3PbI_3$ perovskite components because the lightly fixed $CH_3NH_3^+$ cation in perovskite crystals could be actively converted to CH_3NH_2 with the aid of moisture [38]. As a consequence, the $CH_3NH_3PbI_3$ perovskite was changed to hexagonal PbI_2 with the emission of CH_3NH_2 components owing to its very low boiling point (17 °C), which could be accelerated by a PEDOT:PSS/$CH_3NH_3PbI_3$ perovskite junction. In contrast, the RGO-based devices showed a promising device-stability retaining about 6% (62% of the initial value) of PCE even after 140 h of exposure instead of device failure. The stability of

Table 2 Values for time-resolved PL characteristics by fitting the decay curves of various films.

HTM	ETM	τ_1 (ns)	τ_2 (ns)	Fraction 1	Fraction 2	Average τ (ns)
PEDOT:PSS	-	5.16	47.95	0.26	0.48	45.55
RGO	-	4.44	26.92	0.42	0.32	22.93
PEDOT:PSS	$PC_{61}BM$	2.16	11.11	0.48	0.28	8.89
RGO	$PC_{61}BM$	2.04	8.21	0.67	0.09	4.22

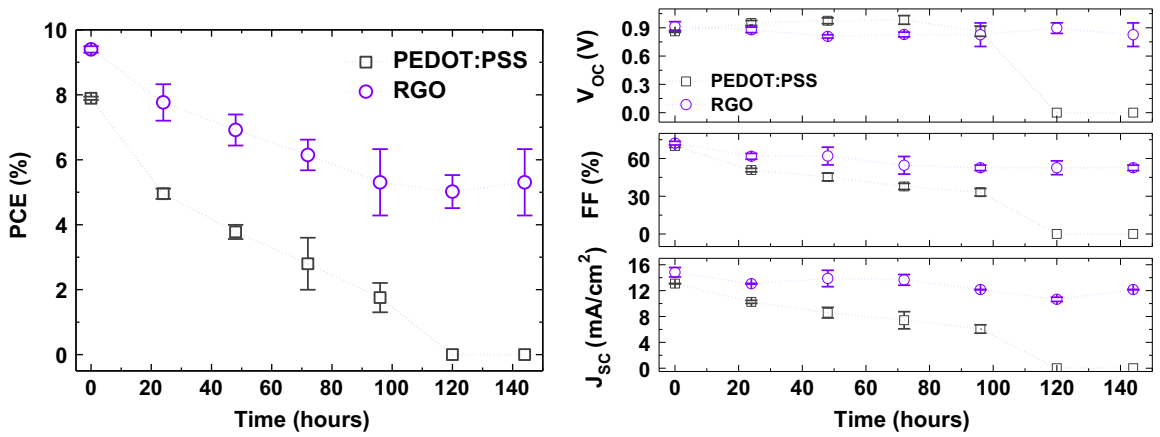

Fig. 4 Variation in the photovoltaic parameters as a function of exposure time to ambient atmosphere for PEDOT:PSS- and RGO-based devices.

devices with RGO stems from the nearly neutral properties of RGO with few surface oxygen functionalities and the inherent passivation ability of RGO against oxygen and moisture, which reduces the decomposition probability of $CH_3NH_3PbI_3$ perovskite films [26,39]. From this point of view, the incorporation of RGO HTMs is more suitable than the conventional PEDOT:PSS HTMs in term of excellent lifetime of PeSCs as well as the advances made in device efficiency.

Conclusions

In conclusion, we have introduced simple solution and room-temperature processed reduced graphene oxide, for the first time, as a novel HTM to guarantee highly efficient and highly stable $CH_3NH_3PbI_3$ PeSCs. The resultant PeSCs with device-architectures comprised of glass/ITO/RGO/$CH_3NH_3PbI_3$/PC_{61}BM/BCP/Ag provided excellent and reproducible device efficiency of up to 10.8%, which was superior to the reference PEDOT:PSS- and GO-based devices. Systematic investigation on the mechanisms of enhancement in photovoltaic characteristics revealed that the improved PeSC performances of RGO devices could be due to the facilitated charge collection with a retarded recombination, high RGO conductivity, better-aligned energy levels, and better growth of the crystalline $CH_3NH_3PbI_3$ phase on RGO HTMs. More importantly, in the ambient stability test, we found that the use of RGO HTMs with the inherent passivation-ability greatly extended the cell-operation time compared to PeSCs employing conventional PEDOT:PSS. These successful demonstrations showed RGO to be an advanced interfacial material to surpass conventional PEDOT:PSS HTMs in terms of photovoltaic performance coupled to device-stability. Also, this approach opens up avenues for research into the design and the development of HTMs, and advances the realization of low cost, solution processible manufacturing, and high-performing PeSCs along with the excellent stability.

Acknowledgments

This work was supported by the National Research Foundation of Korea(NRF) grant funded by the Korea government (MSIP) (No. 2010-0029212), and by the Pioneer Research Center Program (NRF-2013M3C1A3065528), and Basic Science Research Program (2013R1A1A1011880).

Appendix A. Supporting information

Supplementary data associated with this article can be found in the online version at http://dx.doi.org/10.1016/j.nanoen.2014.12.022.

References

[1] M.M. Lee, J. Teuscher, T. Miyasaka, T.N. Murakami, H.J. Snaith, Science 338 (2012) 643–647.
[2] I. Chung, B. Lee, J. He, R.P.H. Chang, M.G. Kanatzidis, Nature 485 (2012)486-489 485 (2012).
[3] H.-S. Kim, C.-R. Lee, J.-H. Im, K.-B. Lee, T. Moehl, A. Marchioro, S.-J. Moon, R. Humphry-Baker, J.-H. Yum, J.E. Moser, M. Grätzel, N.-G. Park, Sci. Rep 2 (2012) 591.
[4] P. Docampo, J.M. Ball, M. Darwich, G.E. Eperon, H.J. Snaith, Nat. Commun 4 (2013) 2761.
[5] M. Liu, M.B. Johnston, H.J. Snaith, Nature 501 (2013) 395–398.
[6] N.-G. Park, J. Phys. Chem. Lett. 4 (2013) 2423–2429.
[7] H.J. Snaith, J. Phys. Chem. Lett. 4 (2013) 3623–3630.
[8] J.H. Heo, S.H. Im, J.H. Noh, T.N. Mandal, C.-S. Lim, J.A. Chang, Y.H. Lee, H.-j. Kim, A. Sarkar, M.K. Nazeeruddin, M. Grätzel, S. I. Seok, Nat. Photonics 7 (2013) 486–491.
[9] H. Zhou, Q. Chen, G. Li, S. Luo, T.-B. Song, H.-S. Duan, Z. Hong, J. You, Y. Liu, Y. Yang, Science 345 (2014) 542–546.
[10] M. Xiao, F. Huang, W. Huang, Y. Dkhissi, Y. Zhu, J. Etheridge, A. Gray-Weale, U. Bach, Y.-B. Cheng, L. Spiccia, Angew. Chem. Int. Ed (2014). http://dx.doi.org/10.1002/anie.201405334.
[11] N.J. Jeon, J.H. Noh, Y.C. Kim, W.S. Yang, S. Ryu, S.I. Seok, Nat. Mater. (2014). http://dx.doi.org/10.1038/NMAT4014.
[12] J.-H. Im, I.-H. Jang, N. Pellet, M. Grätzel, N.-G. Park, Nat. Nanotechnol 9 (2014) 927–932.
[13] J. You, Z. Hong, Y.M. Yang, Q. Chen, M. Cai, T.-B. Song, C.-C. Chen, S. Lu, Y. Liu, H. Zhou, Y. Yang, ACS Nano 8 (2014) 1674–1680.
[14] P.-W. Liang, C.-Y. Liao, C.-C. Chueh, F. Zuo, S.T. Williams, X.-K. Xin, J. Lin, A.K.-Y. Jen, Adv. Mater. 26 (2014) 3748–3754.
[15] J.-Y. Jeng, Y.-F. Chiang, M.-H. Lee, S.-R. Peng, T.-F. Guo, P. Chen, T.-C. Wen, Adv. Mater. 25 (2013) 3727–3732.
[16] S. Ryu, J.H. Noh, N.J. Jeon, Y. Chan Kim, W.S. Yang, J. Seo, S.I. Seok, Energy Environ. Sci 7 (2014) 2614–2618.
[17] E. Edri, S. Kirmayer, S. Mukhopadhyay, K. Gartsman, G. Hodes, D. Cahen, Nat. Commun 5 (2014) 3461.
[18] Y.-H. Kim, H. Cho, J.H. Heo, T.-S. Kim, N. Myoung, C.-L. Lee, S.H. Im, T.-W. Lee, Adv. Mater (2014). http://dx.doi.org/10.1002/adma.201403751.
[19] G. Xing, N. Mathews, S. Sun, S.S. Lim, Y.M. Lam, M. Grätzel, S. Mhaisalkar, T.C. Sum, Science 342 (2013) 344–347.
[20] S.D. Stranks, G.E. Eperon, G. Grancini, C. Menelaou, M.J. Alcocer, T. Leijtens, L.M. Herz, A. Petrozza, H. J. Snaith, Science 342 (2013) 341–344.
[21] J. Seo, S. Park, Y. Chan Kim, N.J. Jeon, J.H. Noh, S.C. Yoon, S.I. Seok, Energy Environ. Sci 7 (2014) 2642–2646.
[22] J.-Y. Jeng, K.-C. Chen, T.-Y. Chiang, P.-Y. Lin, T.-D. Tsai, Y.-C. Chang, T.-F. Guo, P. Chen, T.-C. Wen, Y.-J. Hsu, Adv. Mater. 26 (2014) 4107–4113.
[23] H.-Y. Hsu, C.-Y. Wang, A. Fathi, J.-W. Shiu, C.-C. Chung, P.-S. Shen, T.-F. Guo, P. Chen, Y.-P. Lee, E.-W. Diau, Angew. Chem. Int. Ed (2014). http://dx.doi.org/10.1002/ange.201404213.
[24] Z. Wu, S. Bai, J. Xiang, Z. Yuan, Y. Yang, W. Cui, X. Gao, Z. Liu, Y. Jin, B. Sun, Nanoscale 6 (2014) 10505–10510.
[25] J.-M. Yun, J.-S. Yeo, J. Kim, H.-G. Jeong, D.-Y. Kim, Y.-J. Noh, S.-S. Kim, B.-C. Ku, S.-I. Na, Adv. Mater. 23 (2011) 4923–4928.
[26] J.-S. Yeo, J.-M. Yun, Y.-S. Jung, D.-Y. Kim, Y.-J. Noh, S.-S. Kim, S.-I. Na, J. Mater. Chem. A 2 (2014) 292–298.
[27] Y.-J. Jeon, S. Lee, R. Kang, J.-E. Kim, J.-S. Yeo, S.-H. Lee, S.-S. Kim, J.-M. Yun, D.-Y. Kim, Sci. Rep 4 (2014) 6953.
[28] K.-G. Lim, H.-B. Kim, J. Jeong, H. Kim, J.Y. Kim, T.-W. Lee, Adv. Mater (2014). http://dx.doi.org/10.1002/adma.201401775.
[29] Z. Xiao, Q. Dong, C. Bi, Y. Shao, Y. Yuan, J. Huang, Adv. Mater (2014). http://dx.doi.org/10.1002/adma.201401685.
[30] W.L. Leong, S.R. Cowan, A.J. Heeger, Adv. Energy Mater 1 (2011) 517–522.
[31] J.-S. Yeo, J.-M. Yun, M. Kang, D. Khim, S.-H. Lee, S.-S. Kim, S.-I. Na, D.-Y. Kim, ACS Appl. Mater. Interfaces 6 (2014) 19613–19620.
[32] A. Abrusci, S.D. Stranks, P. Docampo, H.L. Yip, A.K.-Y. Jen, H.J. Snaith, Nano Lett 13 (2013) 3124–3128.
[33] Y. Ogomi, A. Morita, S. Tsukamoto, T. Saitho, Q. Shen, T. Toyoda, K. Yoshino, S.S. Pandey, T. Ma, S. Hayase, J. Phys. Chem. Lett. C 118 (2014) 16651–16659.
[34] O. Malinkiewicz, C. Roldán-Carmona, A. Soriano, E. Bandiello, L. Camacho, M.K. Nazeeruddin, H.J. Bolink, Adv. Energy Mater (2014). http://dx.doi.org/10.1002/aenm.201400345.

[35] J.-S. Yeo, J.-M. Yun, D.-Y. Kim, S.-S. Kim, S.-I. Na, Sol. Energy Mater. Sol. Cells 114 (2013) 104–109.
[36] Q. Chen, H. Zhou, T.B. Song, S. Luo, Z. Hong, H.S. Duan, L. Dou, Y. Liu, Y. Yang, Nano Lett 14 (2014) 4158–4163.
[37] M.O. Reese, S.A. Gevorgyan, M. Jørgensen, E. Bundgaard, S.R. Kurtz, D.S. Ginley, D.C. Olson, M.T. Lloyd, P. Morvillo, E.A. Katz, A. Elschner, O. Haillant, T.R. Currier, V. Shrotriya, M. Hermenau, M. Riede, K.R. Kirov, G. Trimmel, T. Rath, O. Inganäs, F. Zhang, M. Andersson, K. Tvingstedt, M. Lira-Cantu, D. Laird, C. McGuiness, S. Gowrisanker, M. Pannone, M. Xiao, J. Hauch, R. Steim, D.M. DeLongchamp, R. Rösch, H. Hoppe, N. Espinosa, A. Urbina, G. Yaman-Uzunoglu, J.-B. Bonekamp, A.J.J. M. van Breemen, C. Girotto, E. Voroshazi, F.C. Krebs, Sol. Energy Mater. Sol. Cells 95 (2011) 1253–1267.
[38] S. Ito, S. Tanaka, K. Manabe, H. Nishino, J. Phys. Chem. Lett. C 118 (2014) 16995–17000.
[39] H. Yamaguchi, J. Granstrom, W. Nie, H. Sojoudi, T. Fujita, D. Voiry, M. Chen, G. Gupta, A.D. Mohite, S. Graham, M. Chhowalla, Adv. Energy Mater 4 (2014) 1300876.

Jun-Seok Yeo received his undergraduate degree from Sungkyunkwan University in 2009. He is currently a Ph.D. course student supervised by Prof. Dong-Yu Kim at School of Materials Science and Engineering, Gwangju Institute of Science and Technology (GIST). His research is focused on two-dimensional nanomaterials and organic materials for high-performance organic and hybrid solar cells.

Rira Kang received her undergraduate degree from Pusan National University in 2009. Currently she is pursuing her Ph.D. under the supervision of Prof. Dong-Yu Kim at School of Materials Science and Engineering, Gwangju Institute of Science and Technology (GIST). Her research is mainly focused on materials and devices for low-cost and solution-processed organic solar cells.

Sehyun Lee received his undergraduate degree from Sungkyunkwan University in 2011. Currently he is pursuing his Ph.D. under the supervision of Prof. Dong-Yu Kim at School of Materials Science and Engineering, Gwangju Institute of Science and Technology (GIST). His research is mainly focused on organic solar cells using various materials.

Ye-Jin Jeon received her B.S. degree in Department of Materials Science and Engineering from Kunsan National University, and M.S. degree in Department of Flexible and Printable Electronics from Chonbuk National University. She is currently a Ph.D. course student supervised by Prof. Dong-Yu Kim at the Gwangju Institute of Science and Technology (GIST). Her research interests include efficient interlayer for high-performance hybrid and organic solar cells.

NoSoung Myoung received the Ph.D. degree in Physics for his work on the development of mid-infrared solid-state lasers from the University of Alabama at Birmingham, USA, in 2011. From 2011 to 2013, he worked in Samsung Display Co. as a senior research engineer in South Korea. Since 2013, Dr. Myoung is a research fellow in the APRI at the Gwangju Institute of Science and Technology (GIST), South Korea. His main fields of interest include the development and spectroscopic characterization of mid-IR lasers based on semiconductor materials doped with transition metals in quantum system.

Chang-Lyoul Lee received his Ph.D. degree in Materials Science and Engineering from the Gwangju Institute of Science and Technology (GIST), South Korea, in 2003. From 2005 to 2007, he worked as a visiting researcher in Cavendish Laboratory, University of Cambridge. Since 2007, he has worked as a senior and principle researcher in Advanced Photonics Research Institute, GIST. His research interests include optical spectroscopy and optical characterization of organic and conjugated polymer, opto-electronic devices (OLED, OPV) and sensors.

Dong-Yu Kim received his B.S. in chemical technology from Seoul National University in 1986. Also, he received his M.S. in polymer science from Seoul National University in 1988. In 1997, he received his Ph. D. in polymer science/plastic engineering from University of Massachusetts Lowell. Since 1999, he has been at the Gwangju Institute of Science and Technology (GIST), where he is currently a professor in school of materials science and engineering. His current research and interest areas include the organic photovoltaic (OPV), organic light-emitting diode (OLED), organic thin-film transistor (OTFT), azobenzene applications, and synthesis of organic & nano materials.

Jin-Mun Yun received his Ph.D. degree in Materials Science and Engineering from Gwangju Institute of Science and Technology (GIST), South Korea, in 2013. Currently, he is a senior researcher in Radiation Research Division for Industry and Environment at Korea Atomic Energy Research Institute. Currently, his main research interests are focused on two-dimensional nanomaterials and organic-based semiconductors for high-performance organic and hybrid solar cells.

You-Hyun Seo received his B.S. in Department of Electronics Materials Science and Engineering from Chonbuk National University. He is currently a master course student supervised by Prof. Seok-In Na. His current research is organic-inorganic hybrid photovoltaic devices based on perovskite materials.

Seok-Soon Kim received her Ph.D. degree in Materials Science and Engineering from the Gwangju Institute of Science and Technology (GIST), South Korea, in 2006. From 2006 to 2008, she worked as a researcher in GIST. Currently, she is a professor in Department of Nano and Chemical Engineering at Kunsan National University. Her research interests include novel processes and materials for organic & nano material based devices.

Seok-In Na received his Ph.D. degree in Materials Science and Engineering from the Gwangju Institute of Science and Technology (GIST), South Korea, in 2010. From 2009 to 2012, he worked as a researcher and a senior researcher in Korea Institute of Science and Technology. Currently, he is a professor in Professional Graduated School of Flexible and Printable Electronics at Chonbuk National University. His research interests include advanced photoelectronics, novel materials and devices for high-performance solar cells, and flexible and printable electronic devices.